4-16-2016

Algorithms for the Optical Profiling of the Atmospheric Limb Radiometry Data Analysis for the OPAL CubeSat

Eric D. Ashby
Utah State University

Algorithms for the Optical Profiling of the Atmospheric Limb

Radiometry Data Analysis for the OPAL CubeSat

Eric D. Ashby
Mentor: Ludger Scherliess
April 18, 2016

Algorithms for the Optical Profiling of the Atmospheric Limb
By E. D. Ashby

Abstract

The Optical Profiling of the Atmospheric Limb (OPAL) mission is a CubeSat (NSF) project with aims to measure the temperature in the thermosphere between 90 and 140 km. The temperatures are inferred from the characteristic emission lines of molecular oxygen called the O_2 A-band (around 760 nm). These temperatures will be used to better understand the evolution of the upper atmosphere during a solar storm and to analyze the temperature signatures of gravity waves. Multiple steps are required to retrieve temperature data from the OPAL satellite. Initially, the data must be deconvoluted from line-of-sight images. Spectral data must then be converted into temperature data via matching observed emissions with those characteristic of the O_2 A-band.

The software for both the deconvolution and temperature recognition is written in MATLAB. The deconvolution software converts the two-dimensional line-of-sight measurements into a three dimensional distribution by means of the Abel Inversion. The temperature recognition code matches the measured emission curves to the theoretical emission lines (integrated at the spectral resolution of the OPAL instrument, 0.5 nm) to determine the temperature at each altitude in the aforementioned distribution. In the context of developing and testing this software, these two programs are to be combined with further programs—together, simulating the line-of-sight measurement of the atmospheric limb and its emissions by an orbiting satellite—to create a mock mission for the OPAL satellite.

Theory

As most any beginning atmospheric physics student can attest, the atmosphere has multiple layers defined (in part) by the temperature gradient. The first four of these layers are the troposphere, from the Greek *tropos*—change; the stratosphere, from the Latin *stratum*—layer; the mesosphere, the 'middle' layer; and the thermosphere, 'thermo-' referring to heat.[5] In the troposphere and mesosphere, temperature decreases with increasing altitude. However, the temperature *increases* with increasing altitude in the stratosphere and thermosphere.

In the stratosphere, this temperature increase is predominantly due to the absorption of ultra-violet radiation (the ozone layer). In the thermosphere, among other processes, incoming solar radiation splits molecular oxygen into atomic oxygen. Because of the splitting of O_2 in the thermosphere, when viewing the thermosphere from above—as in the case of the OPAL mission—it is fairly safe to assume very little interference in O_2 measurements from higher in the atmosphere (the molecular oxygen density being virtually zero at higher altitudes). It is for this reason that the OPAL mission will be concerned with only those wavelengths in the O_2 A-band between 750 and 780 nm.[2]

Oxygen radiates in the O_2 A-band at different proportions depending on its temperature. These proportions are described by the following equation:

$$S_\lambda(T) = \frac{S_\lambda(T_S)T_S}{T}\exp\left(\frac{1.439E_\lambda''(T-T_S)}{TT_S}\right),^{6} \quad (1)$$

where the S_λ is the emission/absorption line strength at wavelength, λ, and temperature, T. T_S is the standard temperature (~296 K), making $S_\lambda(T_S)$ the line strength at standard temperature, and E_λ'' is the energy of the lower state of the transition. The emission line profiles defined by this equation are characteristic of the temperature and can, therefore, be used to determine the temperature of the

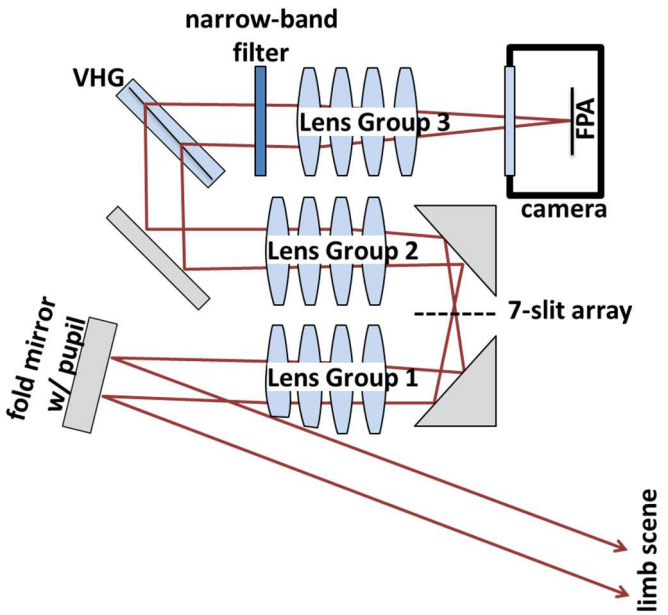

Figure A: Depiction of OPAL instrument set-up.[1-3]

atmosphere through analysis of the air-glow—comparing the expected with the measured.[2] All necessary data can be taken from HITRAN.[7] For an example of the emission lines near standard temperature, see Figure J.

Instrument

The OPAL instrument consists of a Digital Imaging Space Camera (DISC) several mirrors and lens groups, a narrow-band spectral filter, and a holographic grating as shown in Figure A.[1,2] In essence, incoming light enters through an array of seven slits and pass through a volume holographic grating (VHG) and narrow-band filter and is then focused onto the focal plane array (FPA) of the main sensor (DISC).[3] This allows seven vertical samples to be taken, each from a slightly different location.[2]

Each of these samples is broken into its spectral components for spectrographic analysis. This results in seven "rainbow-like" images being focused on the sensor's focal plane array as depicted in Figure B.[2] Altitudinal data can then be inferred from vertical one-pixel strips of these images; spectral data can likewise be inferred from horizontal strips. Horizontal spatial data is obtained by comparing the seven slit images. The instrument has a spectral resolution of 0.5 nm.

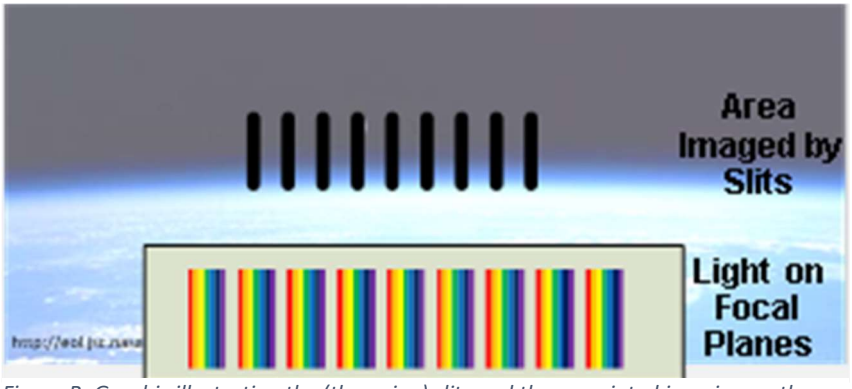

Figure B: Graphic illustrating the (then nine) slits and the associated imaging on the Focal Plane Array.[2]

Procedures

The Abel Inversion

For the OPAL satellite, it being an optical instrument, all data is in the form of light intensity and wavelength. Therefore, in the process of interpreting data, the first obstacle that arises is deconvolution. By nature of the OPAL satellite's tangential LOS, all images contain light from multiple altitudes, as depicted in Figure C.[3,4] This begs the question of how much light is a given altitude is responsible for and how much is interference from above?

The solution to this problem is an occultation or "onion-peeling" method. The idea is to determine the amount of light the topmost layer is responsible for, seeing as how a tangential LOS measurement of said layer would have no interference from below (see Fig. C), and subtract it (scaled appropriately for geometry) from the rest of the data. The process can then be repeated for each successive layer. The method selected for use in the OPAL mission is the Abel Inversion, shown as Equation 2. The variables a, r_{OPAL}, and r are the tangential altitude (perpendicular

$$I(r) = \frac{-1}{\pi}\int_{r}^{r_{OPAL}} \frac{d}{da}\left(S_{LOS}(a)\right)\frac{da}{\sqrt{a^2-r^2}} \quad [4] \tag{2}$$

distance from center of Earth to line of sight s), the altitude of the OPAL satellite, and the target altitude respectively. The inversion of the original LOS measurement S_{LOS} returns a distribution I of intensities as a function of the target altitude r.

In order for any significant amount of data to be processed, the Abel Inversion must be automated. A MATLAB script was written to accomplish this. In order to maintain usefulness, the script was kept as generic as possible—that is, the script simply takes in a projected profile (the measurement) and determines correct three-dimensional distribution associated with it. Testing of the script involved

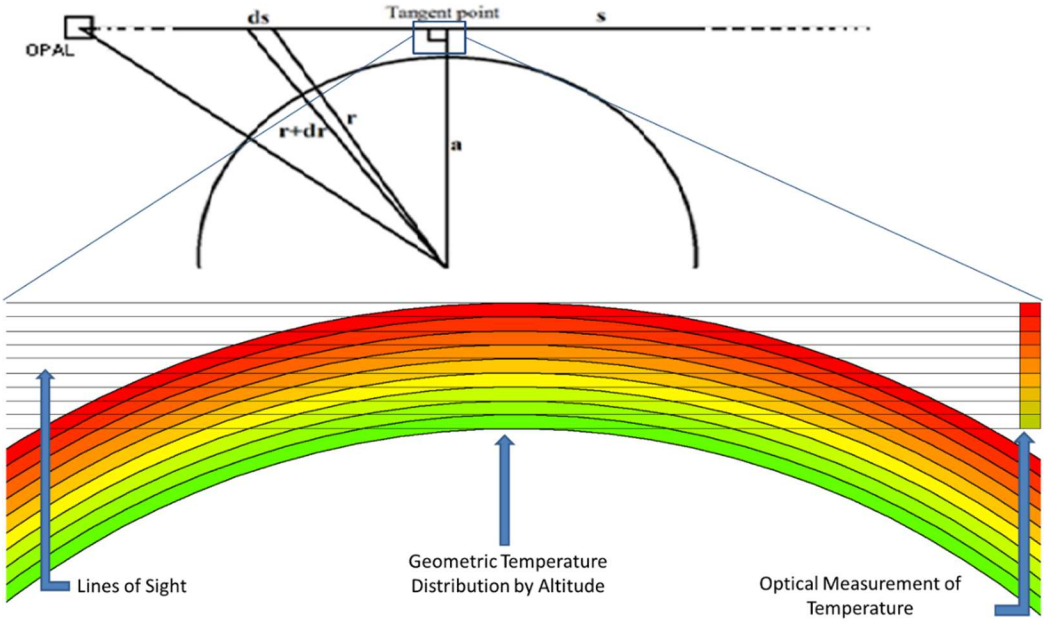

Figure C: Illustration of the convolution of data via tangential LOS measurement.[3,4] Colors represent different temperature emissions (not necessarily a gradient). Notice how the measurement is a sum of emissions along the line of sight. Variable labels are in reference to Eq. 2.

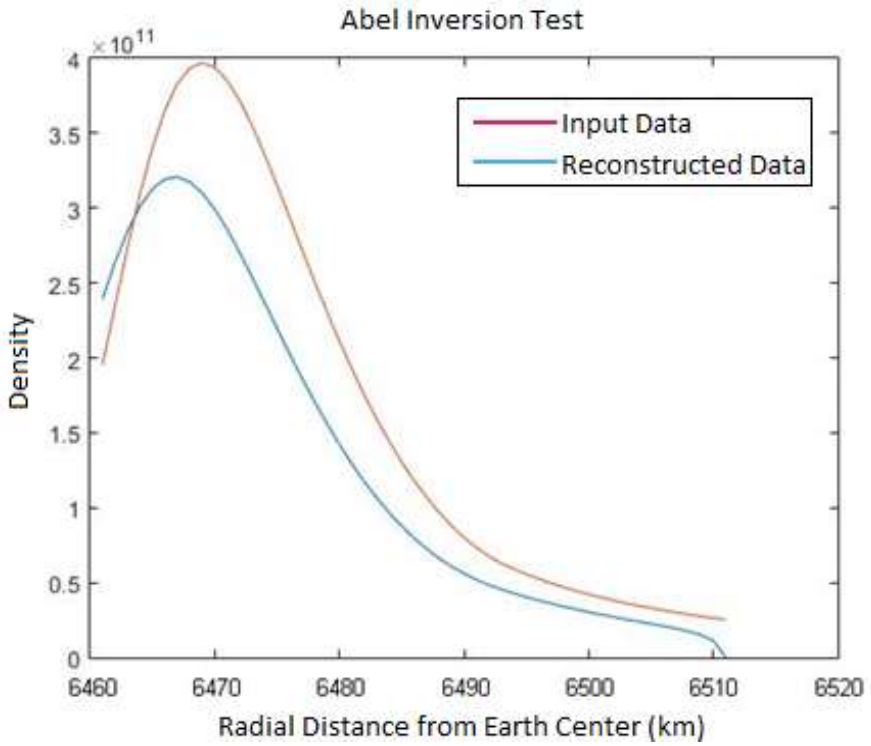

Figure D: Results for early version of the Abel Inversion code. Notice the similar, but ultimately inaccurate, shape of the reconstructed data (blue).

generating a fictitious distribution (taken from MSIS O_2 density distribution data, which is expected to be similar—but not identical—to emission densities), calculating its two-dimensional projection through the use of Equation 3, the Abel Transform (the inverse of the Abel Inversion), and then allowing the script to reconstruct the original distribution.[8] Results are shown in Figure D.

$$S_{LOS}(a) = \frac{-1}{\pi}\int_a^\infty \frac{d}{dr}(I(r))\frac{dr}{\sqrt{r^2-a^2}} \quad [9] \tag{3}$$

As Figure D clearly shows, the software was unable to reconstruct the original distribution with any degree of accuracy. After much consideration, it was determined that it was the model of the LOS measurement, not the inversion, which was to blame. While the inversion could be no better than the resolution of the instrument, the projection (LOS measurement) is not so discretized. After this was realized, the test projection was regenerated at a much higher resolution through the use of a spline. The impressively improved results are shown in Figure E.

Visually, the new results are obviously superior to the previous. To further illustrate the script's accuracy, the percent-of-maximum error was calculated, as shown in Figure F. The increase in error at the high altitudes is due to the mathematically necessary assumption that the density distribution of O_2 tapers off to zero at 140 km. This assumption is approximately true and, in spite of its non-exact veracity, yields an error of less than 7% (6.37% to be exact). A percent error was also calculated (Figure G). However, it is not a good representation of the code's accuracy because of the aforementioned assumption. Percent error calculations will always yield 100% when one of the values is zero and the other is non-zero. Keeping this in mind, the percent error for lower altitudes is still impressive.

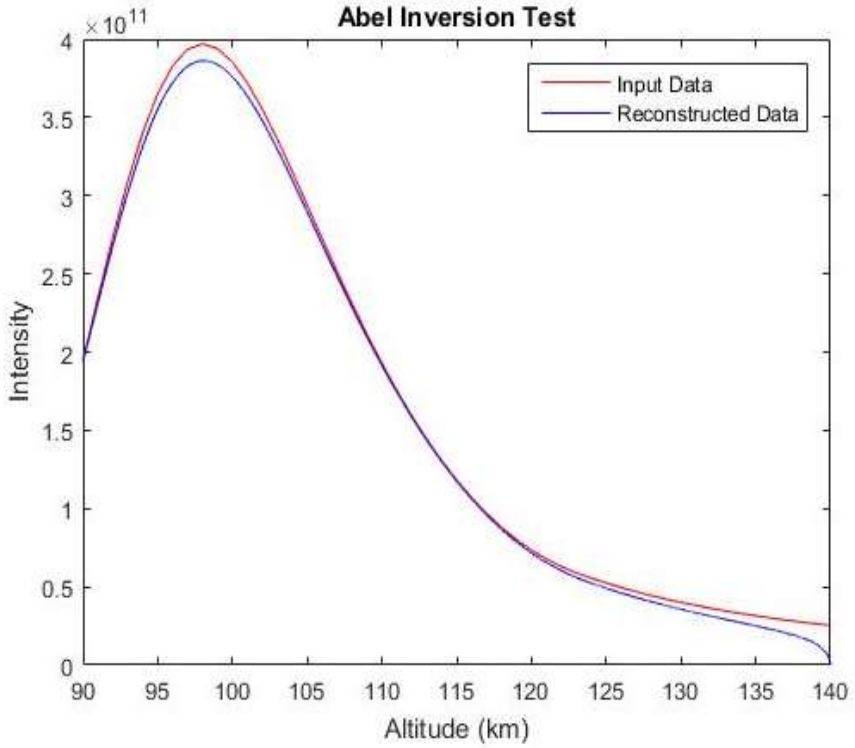

Figure E: Results for the improved code. Note the strong correlation between the two curves.

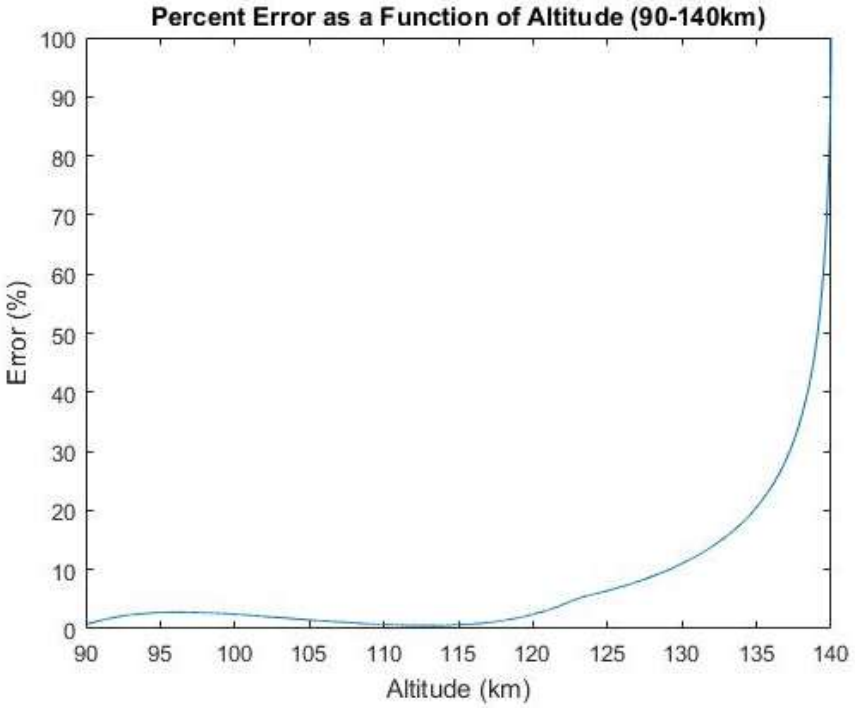

Figure F: Error as a percent of maximum value for the Abel Inversion Test. Note that the increase in error (6.37%) at 140 km is due to the required assumption of zero density at maximum altitude.

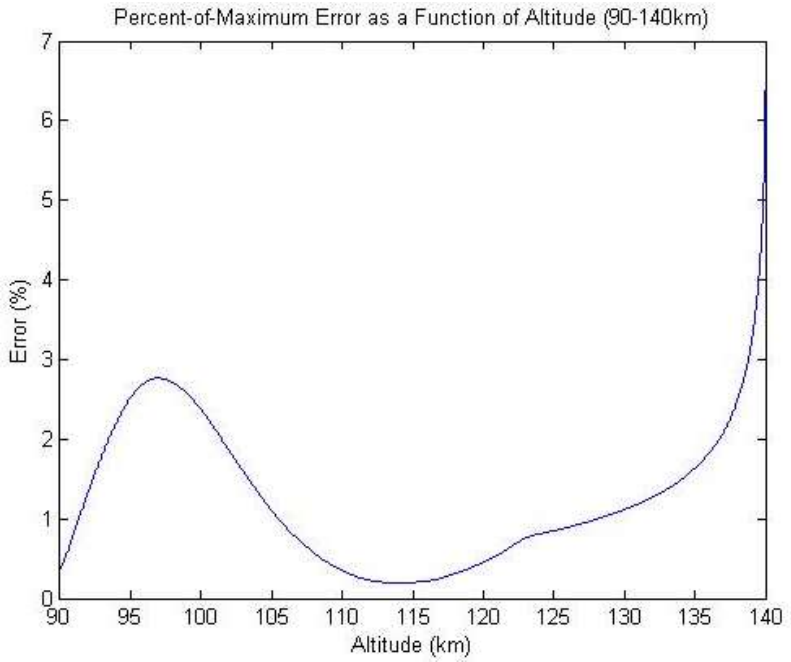

Figure G: Percent error of the Abel Inversion Test. This is not a good indicator of accuracy because of the zero density assumption.

Emission Curves

As mentioned in the theory section, the O_2 emission lines are characteristic of the temperature. However, since the separation of these lines is often less than the OPAL instrument's spectral resolution of 0.5 nm, it is necessary to integrate the emission spectrum at said resolution to obtain a recognizable curve. This was done some time ago by Dr. Andy Christensen, whose results are described in Stephanie Sullivan's master's thesis and are shown in Figure H.[2] In order to have the exact numbers on demand, however, it was decided that the OPAL team should recreate Dr. Christensen's graphs from scratch. To do this, another MATLAB script was written. Emission lines obtained from Eq. 1 are integrated into bins of width 0.5 nm and the results are plotted for comparison to Dr. Christensen's. Results for 150 K are shown in Figure I. When comparing these results with those in Figure H, it should be noted that the OPAL instrument lacks calibration capabilities. Therefore, the exact magnitude of the measured intensities is irrelevant. Any information gleaned from the curves must be based on shape alone. Nevertheless, as is evident, the OPAL team's results are dissimilar Dr. Christensen's.

Results for 297 K are shown in Figure J(i). To illustrate the differences between Fig. J(i) and its counterpart in Fig. H, the ratio of the heights of the two peaks can be compared (while the limitations of this method will be discussed later in the paper, it is sufficient for these purposes). As the figure shows, the ratio of the two peak heights is approximately 1.75. The ratio for Sullivan's graph, though, is about 1.4. It is important to note that near standard temperature (~296 K), Eq. 1 makes no significant changes to the original HITRAN data. It is, therefore, particularly problematic that Fig. J(i) and Sullivan's results do not agree.

Several efforts were made to reconcile this discrepancy. Among them, two stand out as significant. The first was bin shifting. It was noticed that if the wavelength at which the binning process (in the integration) was shifted, the shape of the curve changed. It was reasoned that, if multiple shifts

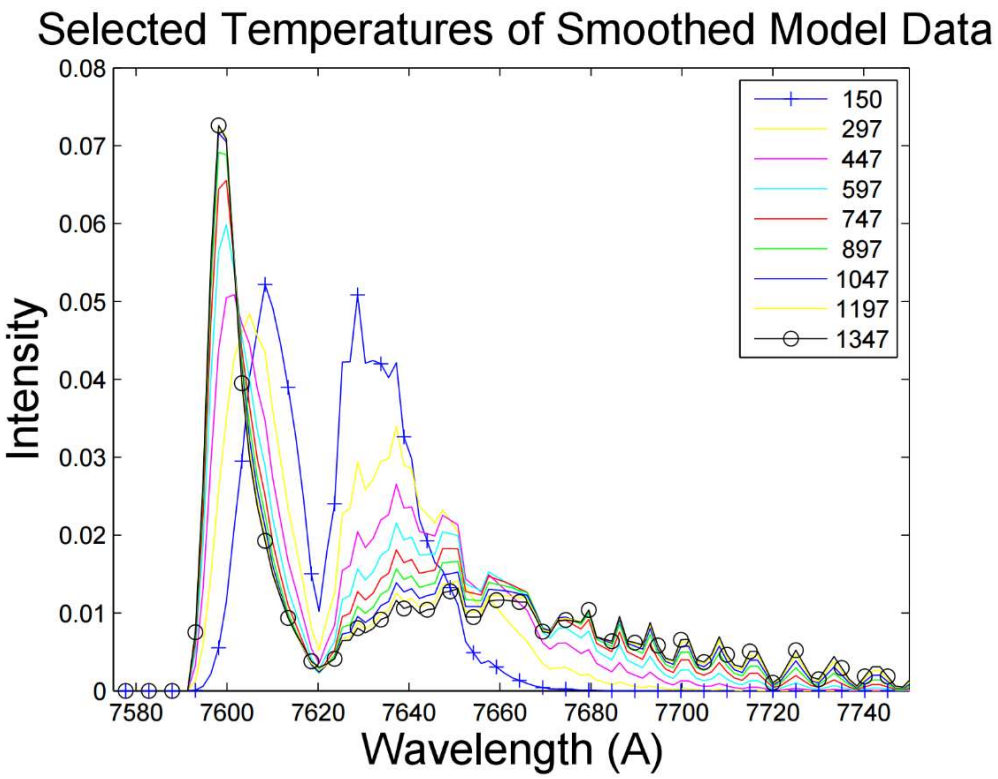

Figure H: Christensen's results as reported by Sullivan.[2,3] Note the curves for 150 K (blue +) and 297K (yellow).

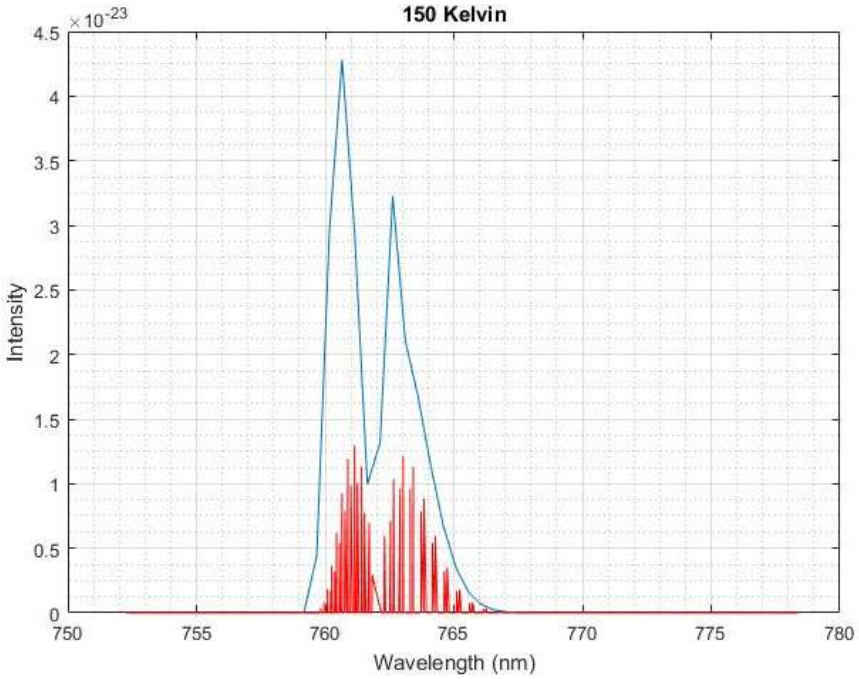

Figure I: Results for 150 K. The integrated emission curve is depicted in blue while the original emission lines are in red. Note how these results do not match those reported by Sullivan.

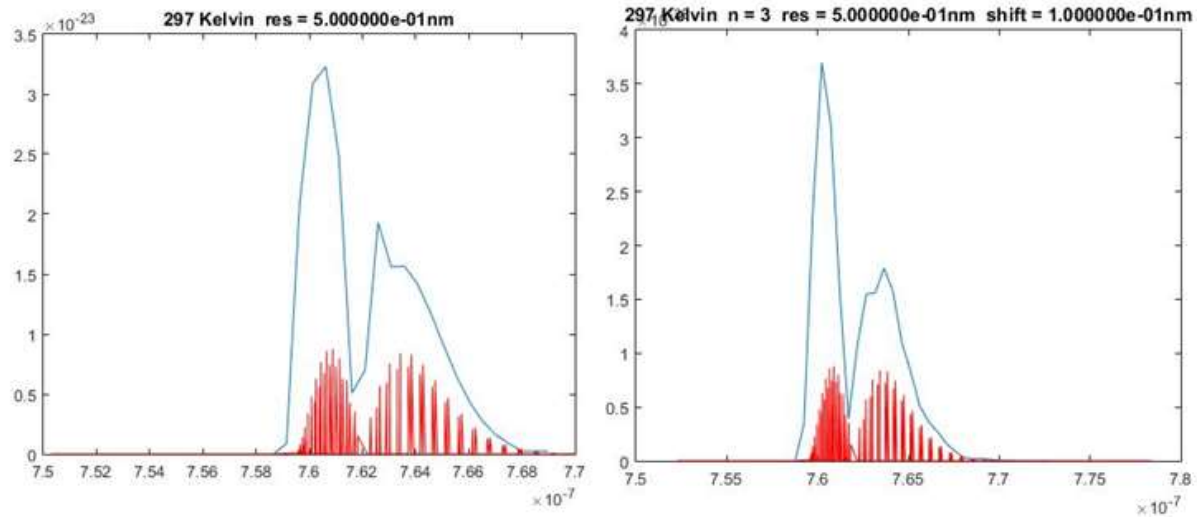

Figure J: (i) Left: Results for 297 K. (ii) Right: Results for 297 K after averaging,

were taken and averaged, the results would more closely match those in Figure H. More code was written for this purpose but results for 150 K were insufficiently changed to warrant being shown here. Instead a comparison of the before and after for 297 K with three .01 nm shifts is shown in Figure J. These results were unsatisfactory, regardless of the number of data sets averaged or where binning started and were typical for the various sizes of shifts implemented. A second solution was proposed: a smoothing algorithm. Code was written to send the data through a boxcar filter (where a central point is averaged with a set number of surrounding points). Results for the minimum boxcar width (three points) are shown in Figure K. Results were again unsatisfactory and larger boxcar sizes were more so.

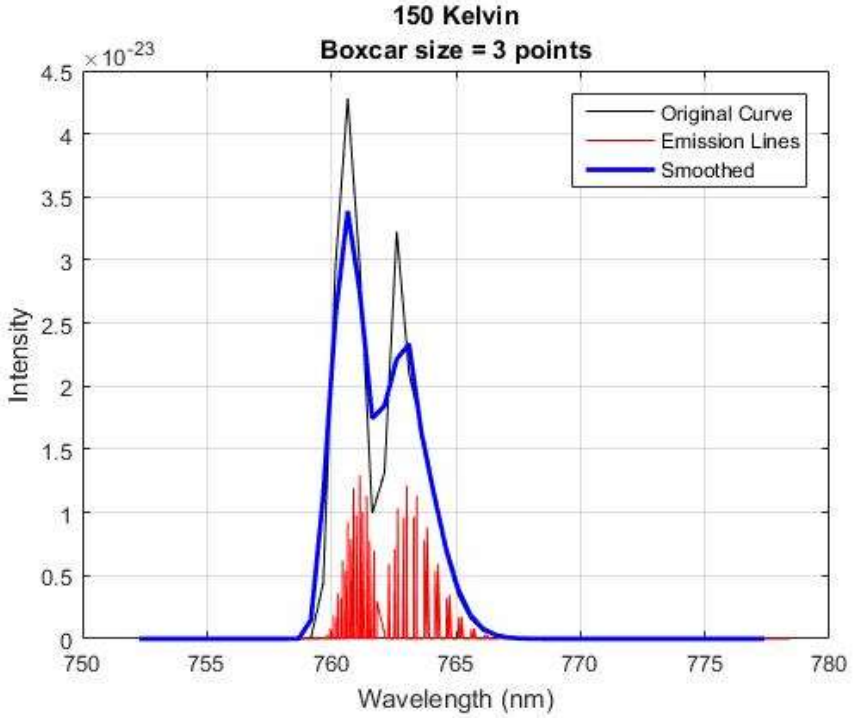

Figure K: Results of boxcar smoothing for the 150 K emission curve.

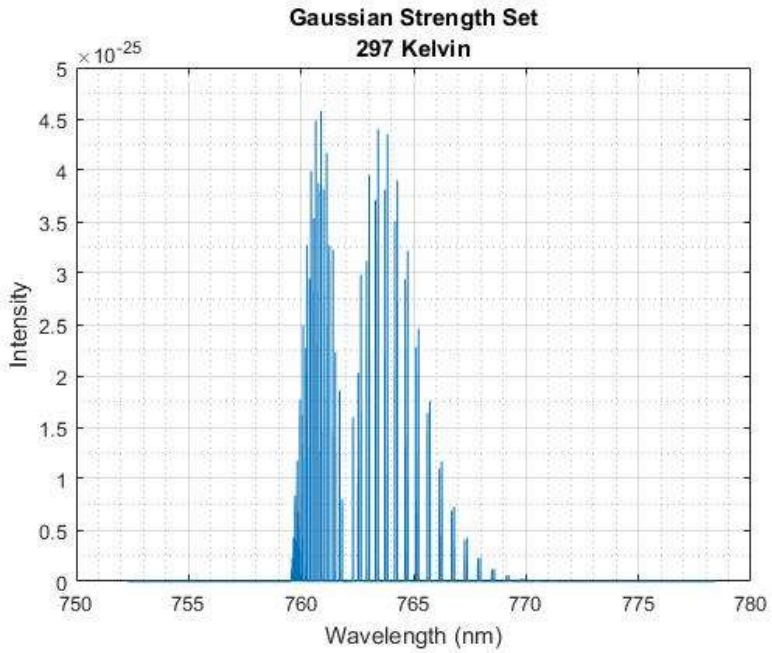

Figure L: The emission line spectrum for 297 K accounting for Doppler broadening.

A third reconciliation effort was to consider Doppler broadening of the emission lines. It was hypothesized that, if the broadening of the lines were wide enough, either no integration would be necessary as the 'emission Gaussians' would overlap to create the same effect or the shape of the integrated lines would be otherwise significantly affected—hopefully so as to agree with Sullivan's graphs. The emission line broadening is given by Equation 4.

$$S(k) = \frac{1}{\alpha\sqrt{\pi}} exp\left[-\left(\frac{k-k_0}{\alpha}\right)^2\right] \mid \alpha = \frac{k_0}{c}\sqrt{\frac{2k_BT}{m}} \quad [6] \tag{4}$$

In the which, k and k_0 are the wave number and target wave number. The temperature is represented by T and c, m, and k_B are the speed of light, the mass of the radiating particle, and Boltzmann's constant respectively.

The implementation of this, did not yield the desired results. Shown in Figure L is the emission line spectrum for 297 K. On close inspection, it was determined that the width (full width at half maximum) of the broadening was approximately 1% or less of the spectral resolution of the OPAL instrument (0.5 nm). An example of one such Gaussian is shown in Figure M. This suggests the broadening of the emission lines is negligible. However, for some temperatures, the emission lines were close enough for their Gaussians or overlap significantly, resulting in one unusually tall spike. This was enough to justify further investigation so the data was sent through the binning algorithm for comparison. Results (Figure N shows a typical outcome) were not closer to those of Sullivan than previous attempts (Fig. J), any variation between Figs. N and J are within the variances due to bin shifting (to be discussed in the next section). That is, results with and without Doppler broadening accounted for were effectively indistinguishable. Therefore, Doppler broadening could not account for the discrepancy.

Interesting to note, are the changes in the Gaussian representations of the emission lines. Specifically, the Gaussians are markedly smaller in amplitude, though relative heights remain virtually

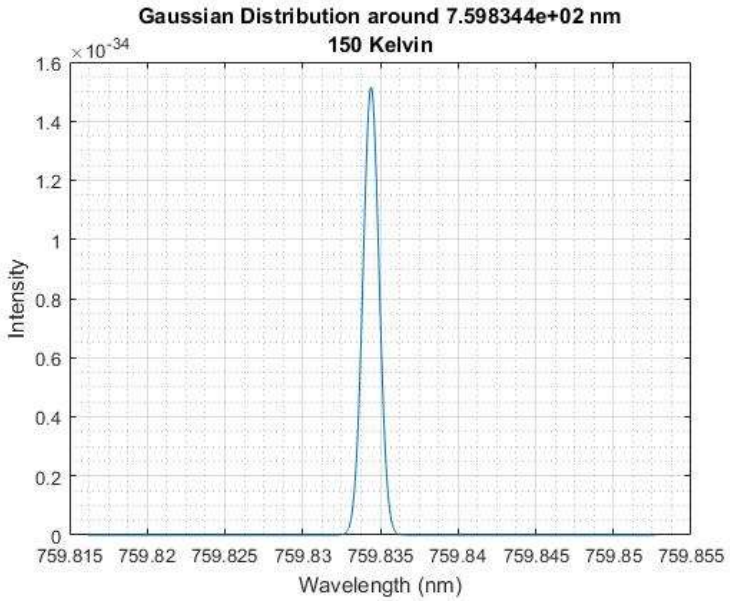

Figure M: One emission line represented by a Gaussian to account for Doppler broadening.

unchanged (except in the aforementioned occasional overlapping of Gaussians). Figure O shows results for 150 K. There is a possible mathematical explanation for this. Presumably, Doppler broadening converts the magnitudes of the emission lines to areas under Gaussian distribution. The theoretical emission lines are infinitely thin, so representations of their magnitudes as areas with even the smallest width must be shorter than the lines' original heights.

This decrease in amplitude is responsible for another interesting effect. Doppler broadening, as Eq. 4 shows, increases with temperature—that is, the width of the Gaussian increases. Combining this concept with that discussed in the preceding paragraph yields the result of higher temperatures having lower amplitudes. This peculiarity can easily be seen in Figure P. It should be noted, however, that this

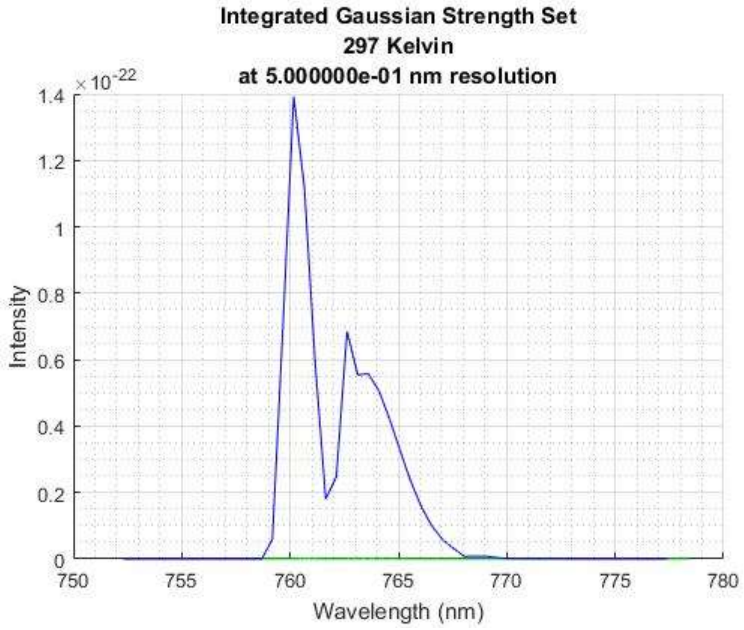

Figure N: Integrated Doppler broadening results.

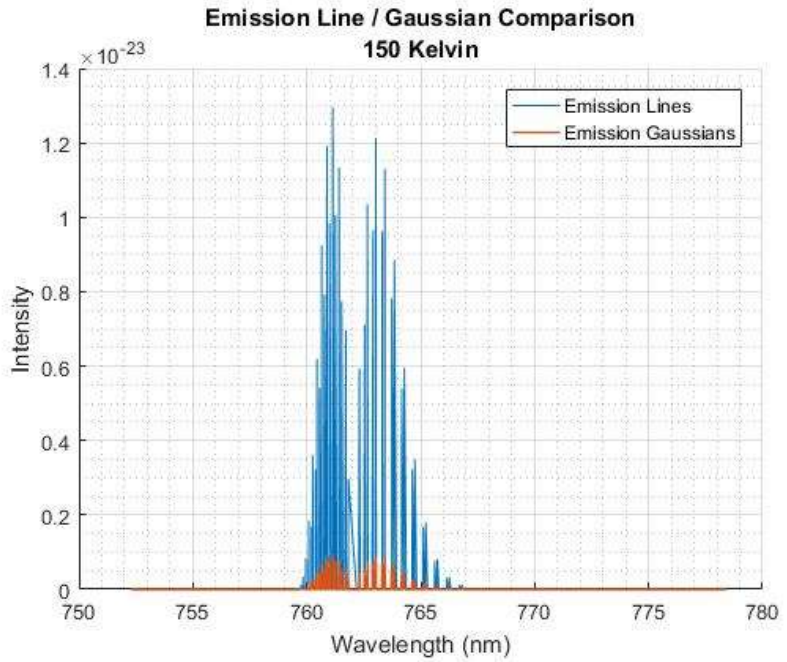

Figure O: Comparison of the amplitudes of the emission lines and Gaussians for 150 K.

does not indicate a dimmer source. Rather, it indicates that the light is simply spread out over more wavelengths.

Variance and Temperature Recognition

Ultimately, the issue of discrepancy was set aside until contact with Dr. Christensen could be made. In the meantime, the OPAL team's efforts to resolve said discrepancy had uncovered another issue. In the original plan, the main parameter to be considered was the relative height of the two

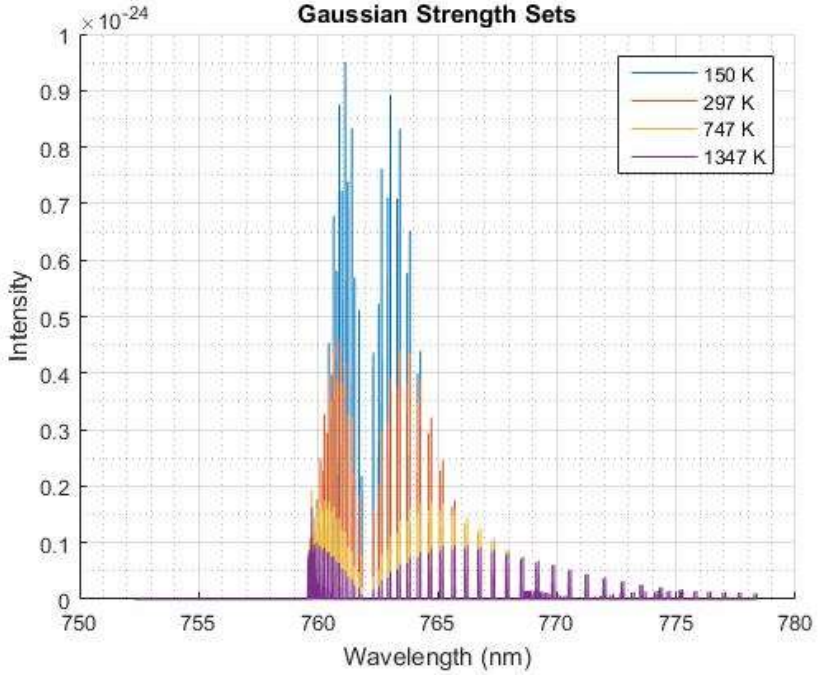

Figure P: Emission lines as Gaussians for a variety of temperatures.

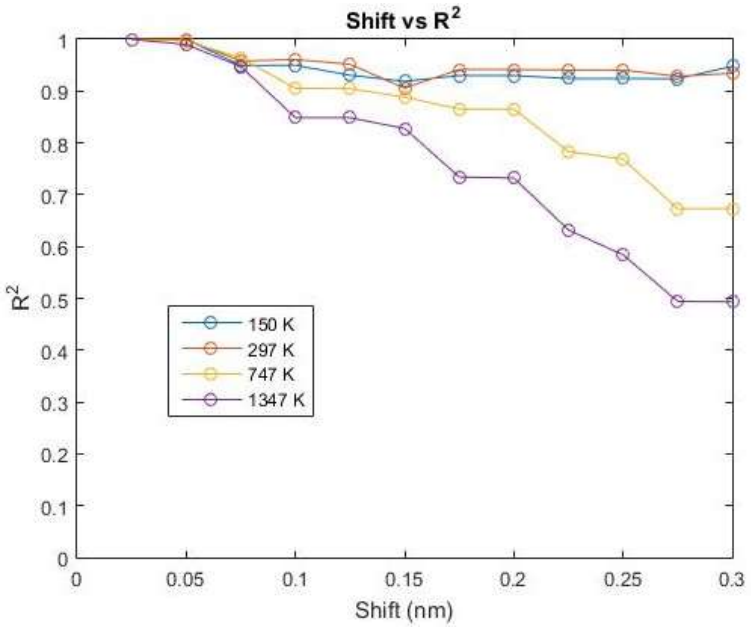

Figure Q: R^2 values of shift (from control) of binning starting point for various temperatures.

peaks (evident in Fig. H, among others). As previously mentioned, experimentation in shifting the binning starting point showed that the shapes of the curves were prone to change. These changes in curve shape were quantized in terms of an R^2 value with respect to a control and are shown in Figure Q. This cast doubt on the accuracy of the planned procedure.

These results begged the question: which parts of the curve are responsible for this error? To answer this, code was written to calculate the root-mean-square (RMS) of the residuals (i.e. the difference from the mean) for the entire curve. Results indicated that the regions around the peaks were to blame as can be seen for 297 K in Figure R. This prompted a closer look at the peaks

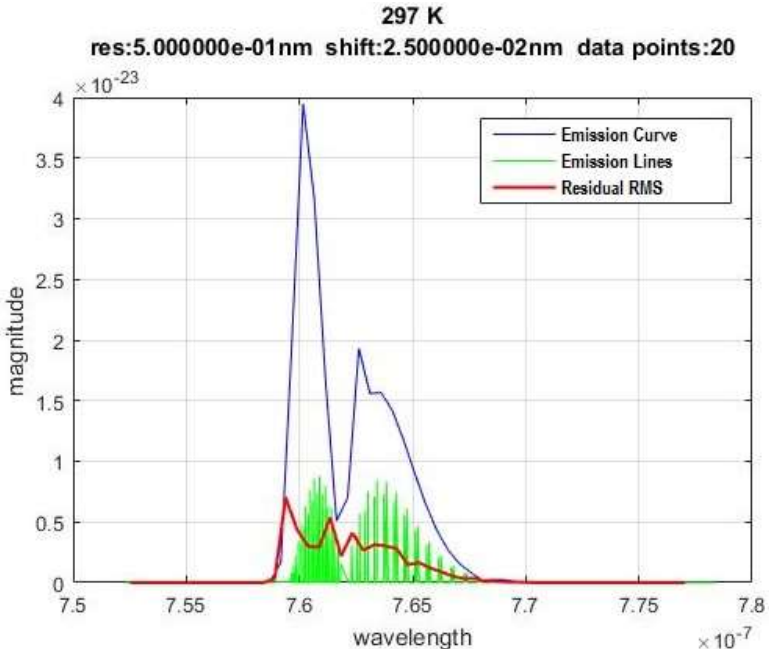

Figure R: Residual RMS plotted against wavelength (calculated from 20 shifts of 0.025 nm).

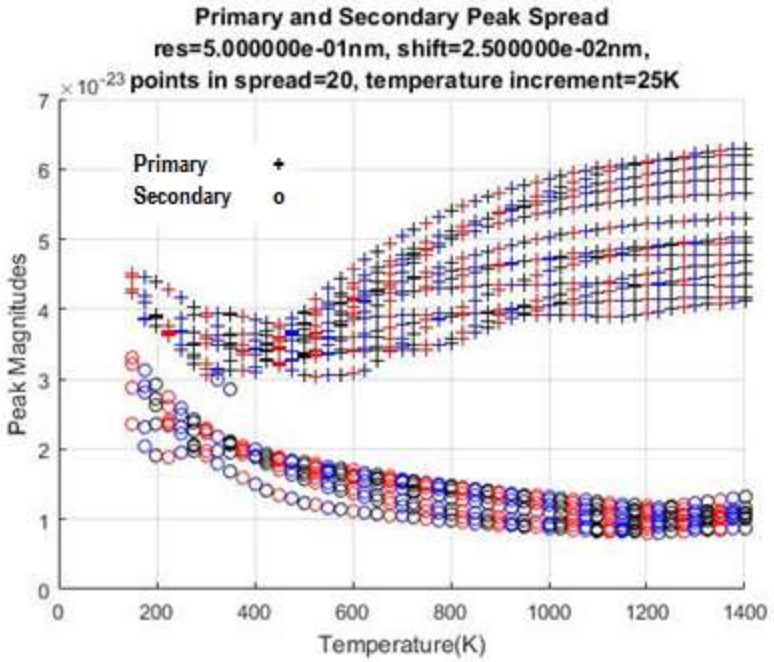

Figure S: Spreads of the primary and secondary peak heights due to bin shifting. Note that the exact units of the magnitude are irrelevant as the OPAL instrument lacks the ability to calibrate for absolute magnitude.

themselves. The spread of possible heights for the primary (left) and secondary (right) peak are shown in Figure S, the RMS of the residuals for each is shown in Figure T, and the spread of the ratio of the primary to secondary is shown in Figure U.

These findings illustrate that using the relative heights of the two peaks alone would result in unacceptable uncertainty in the temperature. That is, the range of temperatures that could yield a given peak ratio are so wide as to render the parameter as effectively non-characteristic of the

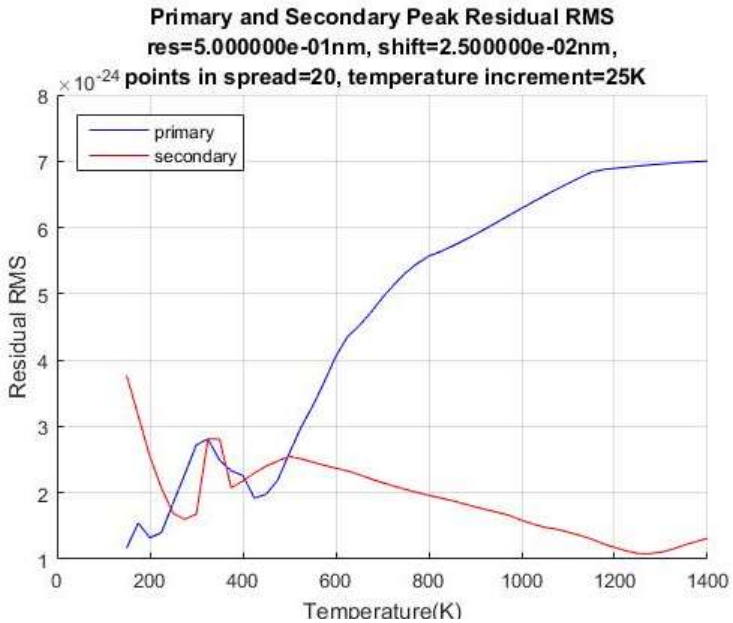

Figure T: The RMS of the residuals for the primary and secondary peaks plotted as a function of temperature.

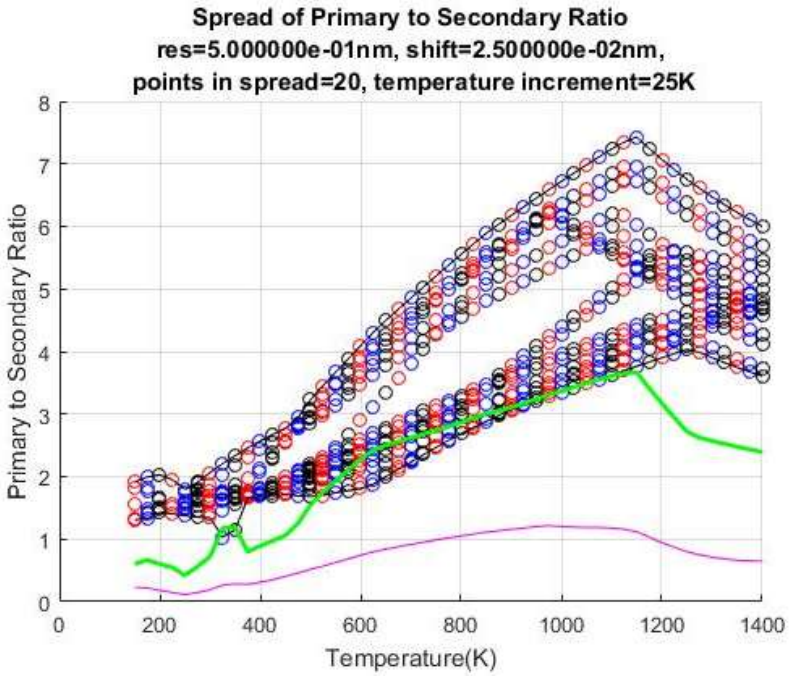

Figure U: The ratio of primary and secondary peak magnitudes formerly thought to be characteristic of the temperature. Also shown at the range (green) and the RMS of the residuals (magenta).

temperatures (at least for the purposes of the OPAL mission). Nevertheless, it was thought that this method could still be used to narrow the range of temperatures to check using other methods of curve comparison. This method still proved to be ineffective as will be discussed later.

One parameter that is less susceptible to bin shifting is the area under the curve. Specifically, we find the total area under the emission curve between two set wavelengths. We then integrate again, bin by bin, looking for the wavelength at which a certain percentage of the total area is reached. Results are promising (especially for 75%) but still show the possibility of error if used independently. That is, this parameter seems to be characteristic (to some extent) of the temperature but yields a resolution that is, while a large improvement over the peak ratio method, still less than satisfactory resolution as illustrated by Figure V. Figure W shows the wavelength range and root-mean-square of the residuals for the previous. Like the peak ratio method, it was thought that the integration method described here could be used to narrow the range of temperatures. It was, therefore, expedient to find yet another comparison parameter. Unlike the peak ratio, integration was projected to be more effective in this capacity.

The apparent discrete nature of the data in Fig. V, while at first alarming, is likely due to the OPAL Instrument's spectral resolution. Further investigation into the issue is beyond the scope of both the intended use of this data and the project, itself. Nevertheless, a superficial investigation was made and it was found that changes in the resolution do apparently correlate with the data's discreteness as evidenced by Figure X.

For a short period, the idea of using the aforesaid technique in conjunction with the peak ratio method was entertained. The idea was to narrow the possible temperature range using both methods,

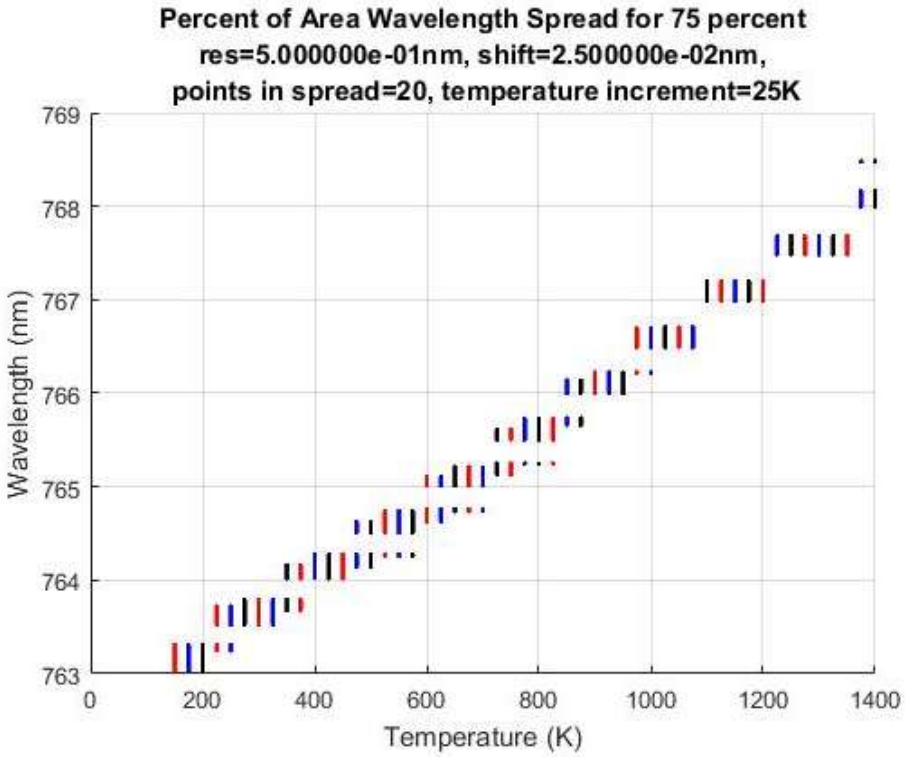

Figure V: Spread of wavelengths (vertical lines) at which the area under the curve reaches 75% of the total vs. temperature. Notice how some temperatures have a presence in more than one wavelength band.

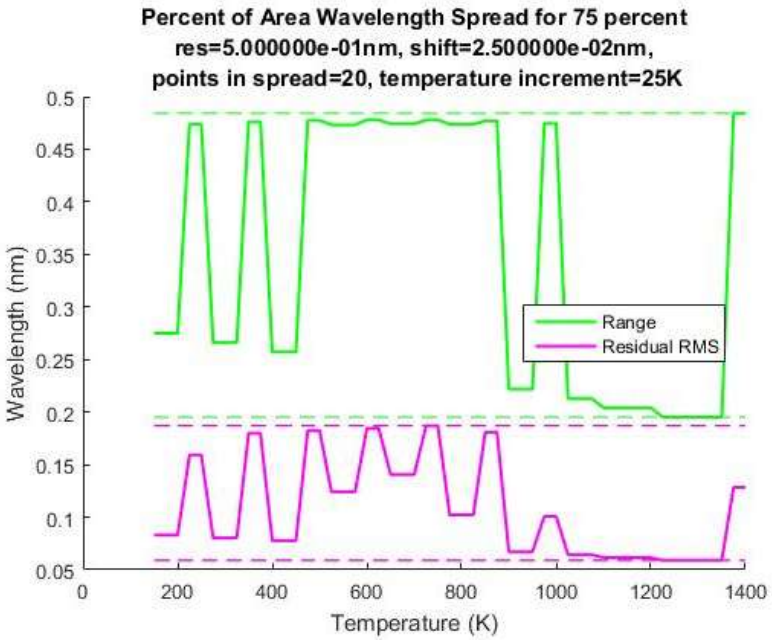

Figure W: The range and residual RMS for the spread in Fig. V with maximums and minimums marked with broken line.

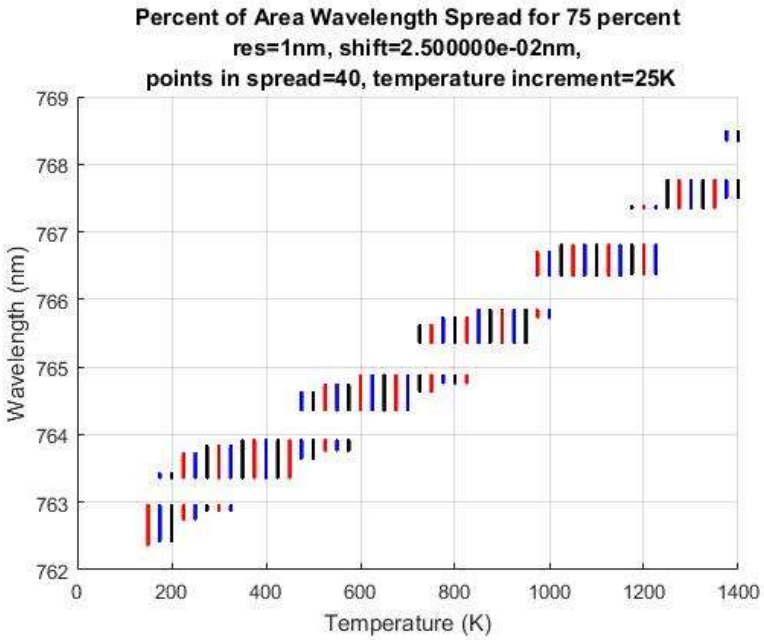

Figure X: The Percent of Area Wavelength Spread calculated with a spectral resolution of 1 nm. Note how the width of the bands (as compared with Fig. V) has increased.

hopefully yielding a desirable resolution. It was quickly determined, however, that including the peak ratio method was unlikely to improve the resolution of the integration method enough to justify it as viable. This fact is evident when a comparison is made between the temperature resolutions in Fig. U and Fig. V. This idea was, therefore, abandoned.

While itself ineffective, work on the peak ratio method suggested one more possible curve comparison technique. In investigating the way in which the primary and secondary peak values change with bin shifting, it appeared that the overall shapes of the curves remain fairly constant. The solution to the comparison problem, it seemed, was to compare the curves point-by-point—the very method the peak ratio was supposed to avoid. Originally, this method was never considered because the OPAL satellite lacks the ability to calibrate its intensity readings. However, calibration may not be necessary.

Previously, calibration was thought to be necessary (in reference to this method) because the uncalibrated observed data would be scaled by some unknown constant. A reference point, possibly an oxygen lamp, could be used to determine the constant, thus allowing for compensation, but (as previously stated) the OPAL satellite is not equipped with such a lamp or any other means of calibration. This may not be an issue if, instead, the comparison is made by taking a ratio of each observed data point to each expected data point. If the ratios are consistently similar, it may be said that the curves are a good match. That is, if the two curves are indeed scaled versions of each other, the ratio of each observed point to each expected point should be the same number: the scaled constant. This fit could be measured by normalizing the ratios (i.e. dividing by the ratio mean) and taking a standard deviation. A small standard deviation indicates a good match.

To further remove sensitivity to bin shifting, each bin shifted version of a given temperature must be considered. To do this, a database of all possible shapes (due to bin shifting) of the emission curves (indexed by their associated temperature) need only be generated once using an adapted version of the very code used to illustrate the shifted shape variability. This database can then be used for quick

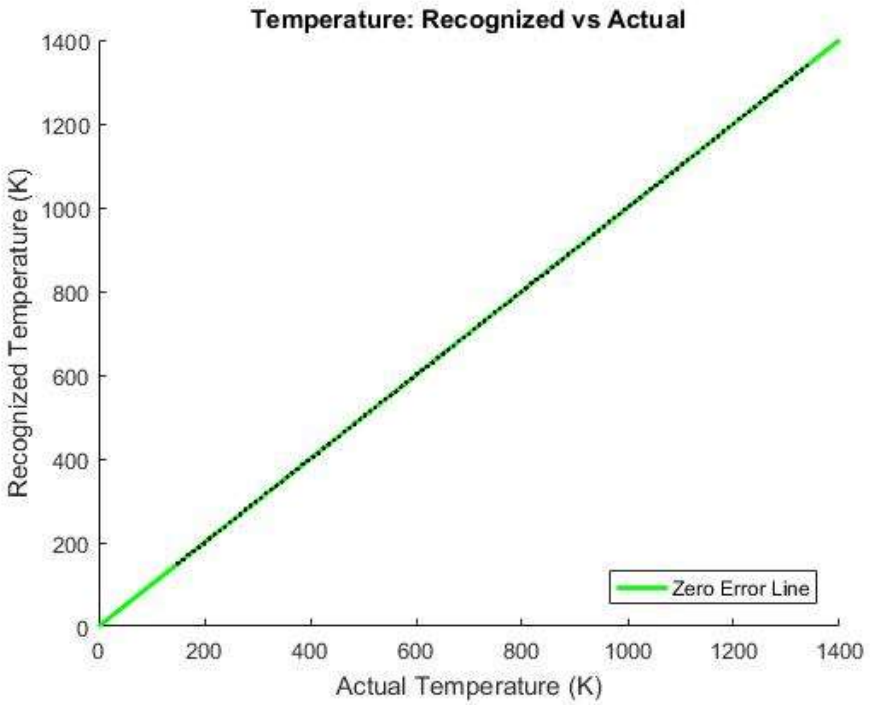

Figure Y: The recognized temperature plotted against the actual temperature. The code was tested with temperatures in increments of 9.8 K so as to check temperatures no already in the database. Black dots indicate results.

calculations. The curve that yields the smallest standard deviation (as described in the previous paragraph) is the closest match. The index of this curve indicates the temperature and emission curve recognition is complete. Results demonstrating the accuracy of this method can be seen in Figures Y and Z.

Peculiar to note is the apparent exponential decrease of the standard deviation of the normalized ratios with increasing temperature (evident in Fig. Z(ii)). As of yet, it is unclear what aspect

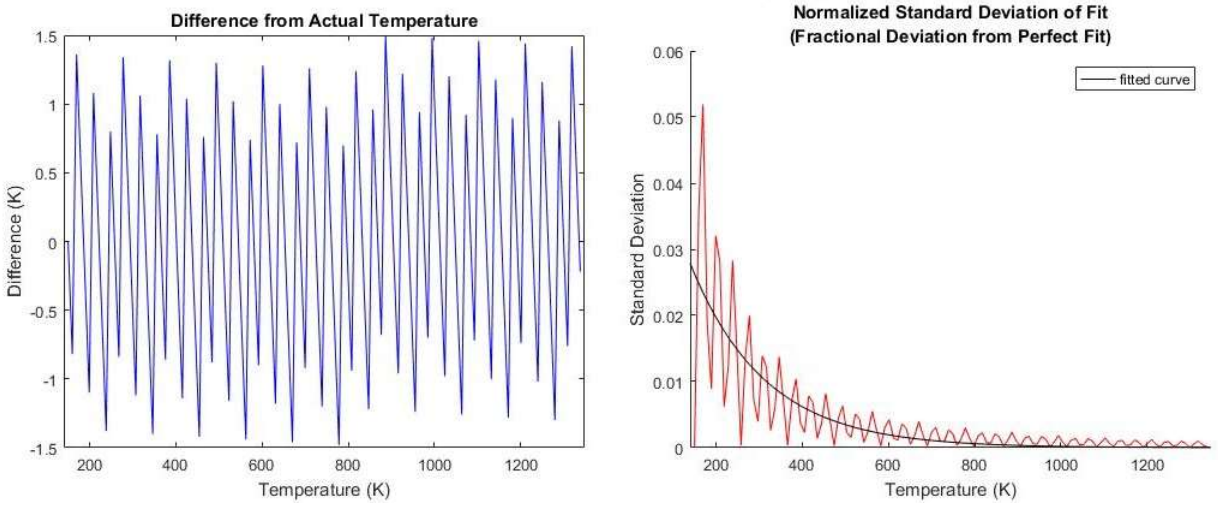

Figure Z: (i) Left: Difference between actual and recognized temperature, indicating that the recognition algorithm selects the closest temperature available in the database.

(ii) Right: Standard deviation of the normalized point-to-point ratios. The oscillation is due to the test temperatures' proximity to temperatures already accounted for in the database. Note the trend line.

of the procedure is responsible for this trend. However, since the trend seems to indicate that the precision of the recognition algorithm improves with increasing temperature *as well* as being acceptable at lower temperatures, the issue has been deemed a low priority and has been set aside for the time being.

With this "brute force" method, computation time may become a concern. If the code could rule out certain temperatures beforehand, though, computation speed could be significantly improved. An attempt to use the peak ratio method as a means of narrowing the range of temperatures to check was made but proved too irregular even before completion. Each ratio value had a temperature range of different width associated with it (as evident in Fig. U). This would mean some curves would take much longer to calculate than others—yielding code with unpredictable running time. The temperature ranges provided by the integration method, however, were much more regular as well as considerably smaller. It was decided that the integration method would be the best means of decreasing computation time and the peak ratio method was abandoned again.

The actual means by which the integration method was used to narrow involved calculating an envelope to uniformly describe which temperatures may be expected to be associated with a certain wavelength. This envelope is determined by applying a linear fit to the data shown in Fig. V (as the wavelength pinpointed by the integration method at 75% seems to increase linearly with temperature), then shifting the line left and right until all data points lie between them. A ten percent buffer was added to either side to allow for variances due to noise. If it so happens that 10% is insufficient, the buffer can always be increased. This envelope is shown in Figure AA. The resolution of this narrowing procedure is superior to that of the emission curve database because it is described by two functions. The narrowing procedure can, therefore, deliver a unique temperature range for any conceivable wavelength.

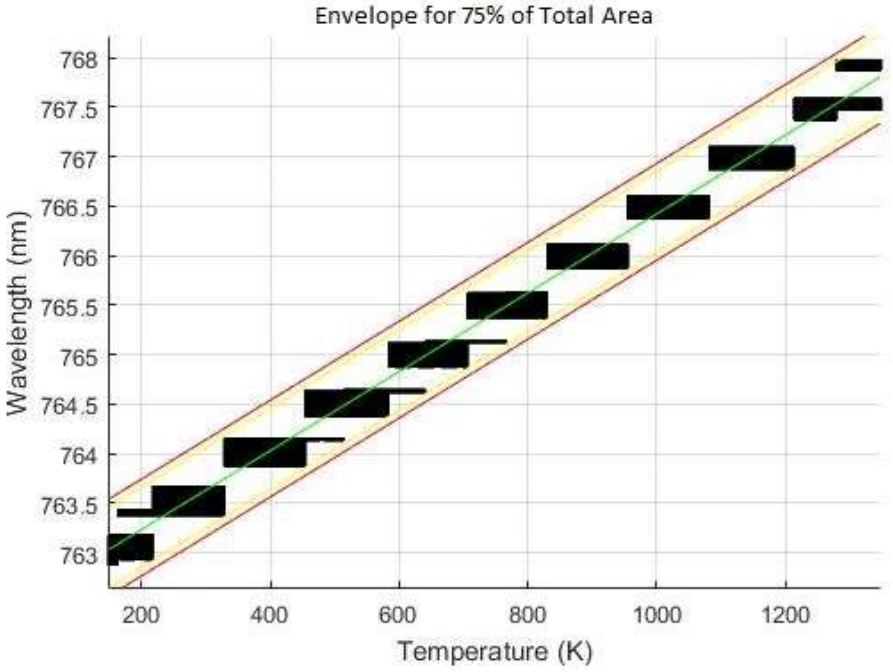

Figure AA: The envelope showing the possible temperatures based on the percentage of total area parameter (used to narrow the search through the temperature database).

Conclusion

The OPAL mission is an ongoing project and there remains much left to do. Still to come, are the integration of the Abel Inversion and the temperature recognition algorithm into one program. This program will then be combined with other programs modelling the upper atmosphere and simulating line-of-sight measurement to create a mock mission for the OPAL satellite. From this mock mission, it will be determined whether the OPAL satellite is capable of. Among other things, the temperature resolution of the system as a whole can be approximated (in a best-case-scenario sense), the satellite's ability to detect gravity waves will be assessed, and the instrument's susceptibility to noise will be studied. The OPAL team is excited to take on these new challenges and hopes to report on them soon.

1 Alan Marchant, Mike Taylor, Charles Swenson, and Ludger Scherliess, "Hyperspectral Limb Scanner for the OPAL Mission," (2014).
2 Stephanie Whalen Sullivan, "Optical sensors for mapping temperature and winds in the thermosphere from a CubeSat platform," Master Thesis, Utah State University (2013).
3 Preston Hooser and Eric Ashby, "The Optical Profiling of the Atmospheric Limb (OPAL) Cubesat Experiment", (Utah State University, 2015).
4 Levan Lomidze, "The Role of Thermospheric Neutral Winds in the Mid-latitude Ionospheric Evening Anomalies," Doctoral Dissertation, Utah State University (2015).
5 "Collins English Dictionary-Complete & Unabridged 10th Edition", (Dictionary.com), Vol. 2015.
6 Patrick Sheese, *Mesospheric ozone densities retrieved from OSIRIS observations of the oxygen A-band dayglow*. Doctoral Dissertation, York University (2009).
7 Laurence S. Rothman, "HITRAN", (Atomic and Molecular Physics Division, Harvard-Smithsonian Center for Astrophysics).
8 Robert McGuire, "MSIS-E-90 Atmosphere Model", (NASA).
9 L. Montgomery Smith, Dennis R. Keefer, and S. I. Sudharsanan, "Abel inversion using transform techniques," Journal of Quantitative Spectroscopy and Radiative Transfer **39** (5), 367-373 (1988).